ISPRS Journal of Photogrammetry and Remote Sensing 156 (2019) 147–159

Contents lists available at ScienceDirect

ISPRS Journal of Photogrammetry and Remote Sensing

journal homepage: www.elsevier.com/locate/isprsjprs

Landslides detection through optimized hot spot analysis on persistent scatterers and distributed scatterers

Ping Lu[a], Shibiao Bai[b,*], Veronica Tofani[c], Nicola Casagli[c]

[a] College of Surveying and Geo-Informatics, Tongji University, Siping Road 1239, Shanghai, China
[b] College of Marine Sciences and Engineering, Jiangsu Center for Collaborative Innovation in Geographical Information Resource Development and Application, Nanjing Normal University, Wenyuan Road 1, Nanjing, China
[c] Department of Earth Sciences, University of Firenze, Via La Pira 4, Firenze, Italy

ARTICLE INFO

Keywords:
Persistent scatterers
Distributed scatterers
Landslides
Optimized hot spot analysis

ABSTRACT

Long-term InSAR techniques, such as Persistent Scatterer Interferometry and Distributed Scatterer Interferometry, are effective approaches able to detect slow-moving landslides with millimeter precision. This study presents a novel approach of optimized hot spot analysis (OHSA) on persistent scatterers (PS) and distributed scatterers (DS), and evaluates its performance on detection of landslides across the Volterra area in central Tuscany region of Italy. 1625 ascending and 2536 descending PS processed from eight years (2003–2010) of ENVISAT images were produced by the PS-InSAR technique. In addition, 16,493 ascending and 9746 descending PS/DS measurement points (MP) processed from four years (2011–2014 for ascending orbits and 2010–2013 for descending orbits) of COSMO-SkyMed images were collected by the SqueeSAR approach. The OHSA approach was then implemented on the derived PS and DS through the analysis of incremental spatial autocorrelation and the Getis-Ord G_i^* statistics. As a result of OHSA, PS and DS MP that are statistically significant with velocity >|±2 mm/year, p-value < 0.01 and z-score >|±2.58 were recognized as hot spots (HS). Meanwhile, a landslide inventory covering the Volterra area was manually prepared as the reference data for accuracy assessment of landslide detection. The results indicate that, in terms of OHSA-derived ENVISAT HS, the detection accuracy can be improved from 23.3% to 25.3% and from 50.7% to 66.4%, with decreased redundancy from 5.3% to 3.7% and from 5.3% to 2.4%, for ascending and descending orbits, respectively. In addition, for OHSA-derived Cosmo-SkyMed HS, the detection accuracy can be improved from 57.7% to 70.3% and from 73.8% to 81.5%, with decreased redundancy from 3.1% to 1.7% and from 3.4% to 2.1%, for ascending and descending orbits, respectively. Compared to traditional HS analysis such as Persistent Scatterers Interferometry Hot Spot and Cluster Analysis (PSI-HCA), OHSA has the significant advantage that the scale distance used for the Getis-Ord G_i^* statistics can be automatically determined by the analysis of incremental spatial autocorrelation and accordingly no manual intervention or additional digital terrain model (DTM) is further needed. The proposed method is very succinct and can be easily implemented in diverse geographic information system (GIS) platforms. To the best of our knowledge, this is the first time that OHSA has been applied to PS and DS.

1. Introduction

Landslide is one of the major types of natural hazards around the world. Italy is a country notably susceptible to landslide hazards. During the last century, due to landslide hazards, more than 5800 deaths and 700,000 homeless people have been caused in Italy (Guzzetti, 2000; Guzzetti and Tonelli, 2004). In addition, it has been estimated that an annual direct economic loss of approximate 12 billion Euros was brought by landslides, accounting for about 0.15% of the national gross domestic product (GDP) throughout the whole country of Italy (Canuti et al., 2002).

As an important branch of remote sensing, spaceborne SAR interferometry (InSAR) is a typical active approach that is able to detect slight surface deformation with millimeter precision at a rather wide coverage (Bamler and Hartl, 1998;Massonnet and Feigl, 1998; Rosen et al., 2000; Hanssen, 2001; Hu et al., 2014; Crosetto et al., 2016). At the beginning stage, such small ground displacement was primarily estimated through differential InSAR (DInSAR). However, DInSAR is often restrained by temporal decorrelation and atmospheric disturbances, both of which are difficult to be thoroughly eliminated when

* Corresponding author.
E-mail addresses: luping@tongji.edu.cn (P. Lu), shibiaobai@njnu.edu.cn (S. Bai), veronica.tofani@unifi.it (V. Tofani), nicola.casagli@unifi.it (N. Casagli).

https://doi.org/10.1016/j.isprsjprs.2019.08.004
Received 8 September 2018; Received in revised form 15 May 2019; Accepted 1 August 2019
Available online 21 August 2019

estimating the representative interferograms of ground deformations. To solve these problems, a long-term InSAR processing approach, generally recognized as Persistent Scatterer Interferometry (PSI), has been developed to extract a quantity of persistent scatterers (PS) point targets, initially based on amplitude analysis and then through phase estimation from a number of temporal SAR images. In past years, several multi-temporal PSI or relevant approaches have been developed such as PS-InSAR (Ferretti et al., 2000, 2001; Colesanti et al., 2003), Interferometric Point Target Analysis (IPTA, Werner et al., 2003; Strozzi et al., 2006), Coherent Pixels Technique (CPT, Mora et al., 2003; Blanco-Sanchez et al., 2008), Stanford Method of Persistent Scatterers (StaMPS, Hooper et al., 2004, 2007), Stable Point Network (SPN, Crosetto et al., 2008; Herrera et al., 2011) and Temporarily Coherent Point InSAR (TCPInSAR, Zhang et al., 2012; Liu et al., 2014). A review of these diverse PSI techniques and their applications can be found in Crosetto et al. (2016).

These PSI approaches have already shown their usefulness in landslide detection. For example, Hilley et al. (2004) analyzed dynamics of slow-moving landslide after it was detected from PS-InSAR outputs. Greif and Vlcko (2012) employed PS-InSAR technique to detect and monitor post-failure landslide deformation in Central Slovakia. Delgado et al. (2011) utilized CPT to detect and monitor unstable slopes in Eastern Betic Cordillera, Spain. Confuorto et al. (2017) utilized both CPT and small baseline subset to analyze the post-failure stage of the Papanice landslide in Italy. Herrera et al. (2009, 2011, 2013) and Notti et al. (2010) implemented SPN to map and monitor the Portalet and the Tena Valley landslides in Central Pyrenees, Spain. Notti et al. (2014) proposed an approach that combines SPN and PS-InSAR for improvement of identifying unstable slopes. Sun et al. (2015a) exploited StaMPS to analyze slope deformation prior to a giant Zhouqu landslide in China. Sun et al. (2015b) operated TCPInSAR technique to detect and further investigate a slow-moving landslide in Oso, USA. This approach was also fulfilled in multi-sensor SAR images to Monitor Zhouqu landslide in China (Sun et al., 2016). Bouali et al. (2018) combined landslide inventory and PSI outcomes to detect landslides across the Palos Verdes Peninsula in California. In addition, after landslide detection, these PSI approaches can be also used in landslide mapping and inventory updating (Lauknes et al., 2010; Righini et al., 2012; Rosi et al., 2018), activity and intensity assessment (Bianchini et al., 2013; Cigna et al., 2013), hazard and risk assessment (Lu et al., 2014a; Oliveira et al., 2015), landslide characterization (Tofani et al., 2013), spatial pattern investigation (Lu et al., 2014b), mechanism interpretation (Colesanti and Wasowski, 2006) and infrastructure damage analysis (Ciampalini et al., 2014; Notti et al., 2015). Furthermore, Bayer et al. (2017) discussed the influence of external DEM on PSI-derived results for landslide study.

Although these long-term PSI techniques are slightly affected by insufficient temporal and geometric correlation, they are commonly limited to individual point-wise scatterers, namely PS. However, for landslide studies, the targeted surface displacements are mostly area-based failures instead of point-based movements. To overcome these limitations, the SqueeSAR technique (Ferretti et al., 2011) has been further developed to extract partially-coherent distributed scatterers (DS) that share homogeneous reflectivity with neighboring pixels in a number of interferometric pairs. That is, the SqueeSAR algorithm jointly processes PS and DS on the basis of their statistical behaviors. Due to the improvement of density and quality of PS/DS measurement points (MP), the SqueeSAR technique may also facilitate the detection of landslides. Compared to the usage of PSI, the SqueeSAR technique is much less reported in current literatures. However, some successful case studies have been reported that DS can be effectively used in landslide detection and further analysis. For example, Bianchini et al. (2015a,b) focused on building deformations in urbanized areas at several landslide-affected sites detected by PS/DS. Raspini et al. (2015) presented the usefulness of SqueeSAR in detecting a large landslide in Montescaglioso, Italy. Also, Carlà et al. (2016) deployed SqueeSAR to improve the landslide susceptibility assessment in the same Montescaglioso area. With the similar objective, Ciampalini et al. (2016) utilized both PS and DS datasets to improve the accuracy of landslide susceptibility map. Intrieri et al. (2018) analyzed DS datasets derived from Sentinel-1 images and additionally employed the Fukuzono model to detect early warning signals of the Maoxiao landslide in western China. Similar to SqueeSAR, Dong et al. (2018) extracted both PS and DS MP to estimate surface displacements of a giant Jiaju landslide in Danba, China. Both of these studies express the potential of the SqueeSAR technique in landslide detection.

The SqueeSAR technique primarily focuses on pixels of SAR images in moderately coherent areas in which surrounding pixels tend to contribute homogeneous reflectivity values as they belong to the same object (Crosetto et al., 2016). Thus, the outcome of SqueeSAR, namely PS/DS MP, can be found not only limited to man-made infrastructures, but also on homogeneous ground surfaces such as uncultivated, desert or debris covered areas (Lagios et al., 2013). As a result, the MP density derived by SqueeSAR can be largely increased. Considering that most current studies for landslide detection through PS and DS are manually analyzed, the increased density of MP may decrease the efficiency of analysis especially over a wide study area. How to efficiently extract useful information from a large dataset of MP for landslide rapid detection remains a practical challenge. Lu et al. (2012) have proposed a semi-automatic analysis of Persistent Scatterers Interferometry Hot Spot and Cluster Analysis (PSI-HCA), a spatial clustering approach based on the Getis-Ord G_i^* statistics, for landslide rapid detection from PS hot spots (HS) at regional scale. Although PSI-HCA has shown its usefulness in landslide rapid detection, its efficiency can often be decreased by the manual determination of scale distance from a digital terrain model (DTM). PSI-HCA shows the advantage that such scale distance for spatially clustering can be estimated from topography. However, the manual intervention may greatly decrease the analyzing efficiency especially for large amount of PS/DS MP. In addition, a DTM with decent resolution is demandingly needed in PSI-HCA, which may often be unavailable over a large area.

To overcome these limitations, this study proposes a novel approach of optimized hot spot analysis (OHSA) on PS and DS, and evaluates its potential in landslide detection in the Volterra area in central Tuscany region of Italy. Compared to PSI-HCA, OHSA has the significant advantage that the scale distance used for the Getis-Ord G_i^* statistics can be automatically determined by the analysis of incremental spatial autocorrelation. Thus, no manual intervention or additional DTM is further needed as in PSI-HCA. To test the usefulness of OHSA in landslide detection, PS processed from eight years (2003–2010) ENVISAT images have been derived by PS-InSAR. Also, PS/DS MP processed from four years (2011–2014 for ascending orbits and 2010–2013 for descending orbits) COSMO-SkyMed images have been achieved by SqueeSAR. Furthermore, a landslide inventory has been manually prepared as the reference data for accuracy assessment of landslide detection. The proposed method is succinct and can be easily implemented in diverse geographic information system (GIS) platforms. To the best of our knowledge, it is the first time that OHSA has been applied to PS and DS.

2. Study area

As shown in Fig. 1, the Volterra Comune is situated in Pisa Province in central Tuscany region of Italy. It is strongly affected by landslide hazards especially in the southwestern areas of the Volterra city, which lies on the top of a narrow plateau or tableland at an elevation of about 550 m. The geological background of the Volterra Comune is chiefly made up of a Pliocene marine sedimentary succession, with the bottom stratigraphic layers of marine clays of Early-Middle Pliocene age overlapped by cemented sandy deposits, and the top stratigraphic layers of the calcarenites of Volterra limestones that feature the end of this sedimentary succession (Bianchini et al., 2015b; Pratesi et al.,

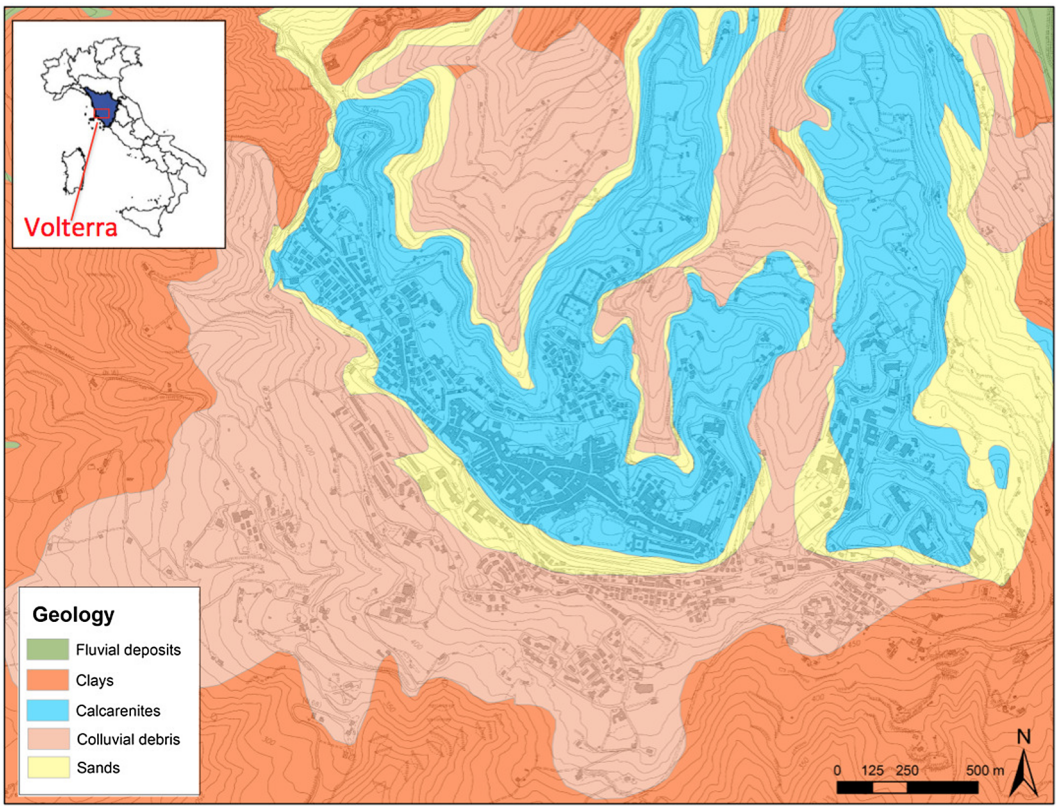

Fig. 1. The geographic location and the geological settings of the Volterra area.

2015). The detritus of fine and coarse sediments, formed in lacustrine cycles or in continental fluvial-deltaic processes, can also be recognized in this area (Bianchini et al., 2016). The Pliocenic (Zanclean-Middle Piacentian) sandy-clayey formations accumulated by those clays, sands and calcarenites in horizontal or sub-horizontal layers from southwest to northeast with an inclination of less than 10 degrees, and their stratigraphic differences in geotechnical characteristics may induce a number of landslides that distribute in those steep cliffs surrounding the plateau (Terrenato, 1998; Sabelli, 2012; Bianchini et al., 2015b; Pratesi et al., 2015). In Volterra, intensive rainfalls often occur in spring and autumn due to the humid Mediterranean climate (Bazzoffi et al., 1997), and may accelerate slope movements in these clayey and poorly-vegetated hillslopes. In addition to heavy rainfall, the freezing-thaw cycles may also trigger landslides and other rapid geomorphological processes such as soil erosion (Nolesini et al., 2016). A landslide inventory map has been produced and lately updated by the Tuscany region authority in 2012, based on field surveys, aerial photos, geological maps and topographic maps at a scale of 1:10,000. The inventory map shows that the major types of landslides occurred in Volterra are translational slides and flows with shallow mass movements.

3. Datasets and methodology

PS derived from eight years of C-band ENVISAT images spanning from February 2003 to July 2010 were achieved using a multi-interferometric approach of PS-InSAR technique (Ferretti et al., 2000, 2001) processed by Tele-Rilevamento Europa (TRE). As indicated in Table 1, 41 and 35 scenes of ENVISAT images were processed for ascending and descending orbits, respectively. The temporal coverage is from 26 August 2003 to 20 July 2010 for ascending images and from 10 February 2003 to 28 June 2010 for descending acquisitions. These images were captured at an Advanced Synthetic Aperture Radar (ASAR) beam mode of IS2 that provides a ground range resolution of approximate 24 m. Defining a coherence value higher than 0.65, 1625 ascending and 2536 descending PS were finally obtained, with an estimated geocoding accuracy of 10 m in east–west and 5 m in north–south directions. The PS velocity was then calculated along line-of-sight (LOS) with estimated standard deviations ranging from 0.1 to 2 mm/year depending on the deviation of motion from the linear model and additionally the coherence and distance to the reference point.

Furthermore, PS/DS MP were extracted from four years of X-band COSMO-SkyMed images based on the SqueeSAR algorithm, an approach developed by TRE that extracts not only point-wise deterministic objects but also distributed scatterers from all possible interferograms, namely squeezing all possible ground targets within the acceptable coherence to estimate optimum phase values (Ferretti et al., 2011). As indicated in Table 1, a total of 41 ascending and 25 descending COSMO-SkyMed images were utilized for the SqueeSAR processing, with the beam mode of 01 and 04, respectively. These images were captured with the imaging mode of H4 that renders a ground resolution of 3 m. The relative orbit is T150 for ascending and T113 for descending images. The incidence angle is 26° and 31° for ascending and descending orbit, respectively. The temporal coverage is from 28 January 2011 to 20 January 2014 for ascending acquisitions and from 24 February 2010 to 15 November 2013 for descending images. The SqueeSAR approach firstly created a window centered on each single pixel of the COSMO-SkyMed image. This pixel was subsequently compared with those adjacent pixels using the nonparametric Kolmogorov–Smirnov (KS) test. A group of homogenous pixels having similar signals were thus created as a DS, identified by this KS test based on the maximum absolute difference between two cumulative distribution functions. Heterogeneous adjacent pixels with non-similar signals, namely with different distribution functions during the KS test, were accordingly discarded (Carlà et al., 2016). Finally, the selected DS were jointly processed with PS based on the traditional PS-InSAR approach to derive PS/DS MP and estimate their time series displacements. In the Volterra area, a total of 16,493 and 9746 PS/DS MP were finally obtained from ascending and descending orbit, respectively. The PS/DS

Table 1
A summary of the processed SAR images and derived PS/DS datasets.

Sensor	Radar Band	Wavelength	Passing Mode	Beam Mode	Ground Range Resolution	Number of Scenes	Temporal Coverage	Processing Technique	Number of PS/DS MP
ENVISAT ASAR	C-Band	5.66 cm	Ascending	IS2	24 m	41	26 August 2003–20 July 2010	PS-InSAR	1625
ENVISAT ASAR	C-Band	5.66 cm	Descending	IS2	24 m	35	10 February 2003–28 June 2010	PS-InSAR	2536
COSMO-SkyMed	X-Band	3.12 cm	Ascending	01	3 m	41	28 January 2011–20 January 2014	SqueeSAR	16,493
COSMO-SkyMed	X-Band	3.12 cm	Descending	04	3 m	25	24 February 2010–15 November 2013	SqueeSAR	9746

velocity was evaluated along LOS with estimated standard deviations ranging from 0.1 to 2.0 mm/year.

OHSA was then carried out on the georeferenced PS derived from ENVISAT images and PS/DS MP extracted from COSMO-SkyMed images for analyzing their spatial clustering tendencies. The approach was implemented in the Spatial Statistics Tools in ArcGIS v10.7. The flowchart of OHSA is illustrated in Fig. 2.

The first step is PS/DS data assessment and aggregation. The purpose is to ensure that OHSA has adequate number and variation of the analyzed datasets. The PS/DS MP were input into ArcGIS with velocity as the analyzing field for OHSA. The average nearest neighbor (ANN) distance of each MP was calculated and the distribution of all ANN distances were evaluated. PS/DS MP with standard deviation $>3\sigma$ from their closest noncoincident neighbors were considered as locational outliers to be excluded from OHSA. Based on the calculated ANN and the median nearest neighbor (MNN) distance, the remaining PS/DS MP were further converted to velocity-weighted points.

The next step is the analysis of incremental spatial autocorrelation. The purpose is to automatically determine the scale distance d for the Getis-Ord G_i^* statistics, which used to be an uncertain step in traditional HS analysis. An effective approach for defining the pronounced scale distance is to consider the statistic nature of datasets based on the distance where high spatial autocorrelation can be found, and it can be usually fulfilled by employing an iterative and data-driven process that determined how spatial autocorrelation varies at different distances (Peeters et al., 2015). As a result, the spatial autocorrelation was estimated by the global Moran's I index defined as follows (Sato, 2014; ESRI, 2017):

$$I = \frac{n}{S_0}\frac{\sum_{i=1}^{n}\sum_{j=1}^{n} w_{ij}(x_i-\bar{x})(x_j-\bar{x})}{\sum_{j=1}^{n}(x_j-\bar{x})^2} \quad (1)$$

Here n is the total number of PS/DS MP. $\bar{x}$ is the mean velocity of derived PS/DS. w is the spatial weight and S_0 is sum of all spatial weights as:

$$S_0 = \sum_{i=1}^{n}\sum_{j=1}^{n} w_{ij} \quad (2)$$

From the outcomes of the global Moran's I index, the z-score used to determine the significance level of spatial autocorrelation is accordingly measured as:

$$z = \frac{I - E[I]}{\sqrt{Var[I]}} \quad (3)$$

where $E[I]$ and $Var[I]$ are calculated as:

$$E[I] = -1/(n-1) \quad (4)$$

$$Var[I] = -E[I^2] - E[I]^2 \quad (5)$$

Based on the z-score calculated by Eq. (3), the spatial autocorrelation was incrementally estimated at each scale distance. The pronounced scale distance utilized in the subsequent Getis-Ord G_i^* statistics was finally selected as the distance where the peak z-score locates (Fig. 2).

The third step is to perform the Getis-Ord G_i^* statistics (Getis and Ord, 1992, 1996; Ord and Getis, 1995), a local statistic model that quantifies the degree of spatial dependence in the pronounced scale distance derived above. The G_i^* statistics was implemented to determine the clustering level of PS/DS MP, specifying a single MP at a location i and its neighbors j within a searching distance d. For each single MP at a site i, the G_i^* index can be estimated as:

$$G_i^*(d) = \frac{\Sigma x_j + x_i - n_{ij}\times\bar{x}^*}{\sqrt{s^*\{[(n\times n_{ij}) - n_{ij}^2]/(n-1)\}}} \quad (6)$$

Here n is the total number of PS/DS MP; n_{ij} is the number of PS/DS MP within the scale distance d; x is the surface displacement recorded by PS/DS, x^* and s^* are respectively the mean value and the standard deviation of all displacements that are revealed by the whole PS/DS MP. Through this Getis-Ord G_i^* statistics, clustered and random patterns can be separately identified. The outcomes of the Getis-Ord G_i^* statistics for each PS/DS MP are the calculated values of z-score (standard deviation) and p-value (independence probability), both of which are utilized to estimate the statistical significance of spatial autocorrelation. In particular, for each PS/DS MP the z-score was utilized to indicate statistical significance of clustering at 90% (p-value = 0.10), 95% (p-value = 0.05) and 99% (p-value = 0.01) confidence level, corresponding to a z-score value of ±1.65, ±1.96 and ±2.58, respectively (Fig. 2). Positive and negative z-scores indicate spatial clusters of PS/DS moving towards and away from LOS, respectively.

The final step is to determine HS. In this study, the threshold of p-value and z-score to determine the clustered pattern was set as 0.01 (99% confidence level) and |±2.58|, respectively. PS/DS MP with velocity ⩽|2| mm/year were discarded from OHSA because the standard deviations of estimated velocity are up to 2 mm/year. In consequence, PS/DS MP with velocity >|±2| mm/year, p-value < 0.01 and z-score > |±2.58| were defined as HS.

To evaluate the usefulness of OHSA on PS/DS for landslide detection, the landslide inventory prepared by the Tuscany region authority was selected as the reference data. This landslide inventory was produced and updated in polygon in GIS based on field surveys, aerial photos, geological maps and topographic maps at a scale of 1:10,000. The accuracy assessment was then conducted by detection accuracy and redundancy for PS/DS and HS, respectively.

4. Results

The PS-InSAR technique has extracted 1625 and 2536 PS from the processed ascending and descending ENVISAT images, respectively. Those PS are prevalently recognized on man-made objects such as buildings, infrastructures and roads in the urbanized area in Volterra. Among them, 215 ascending and 428 descending active PS with velocity >|±2| mm/year were obtained. An overview of the derived PS from the ENVISAT imageries is illustrated in Fig. 3. The positive and negative velocity values indicate the moving direction towards and away from the satellite, respectively.

The SqueeSAR approach has generated 16,493 and 9746 PS/DS MP from the processed ascending and descending COSMO-SkyMed images, respectively. Among them, 1120 ascending and 1082 descending active MP with velocity >|±2| mm/year were mapped. In addition to buildings,

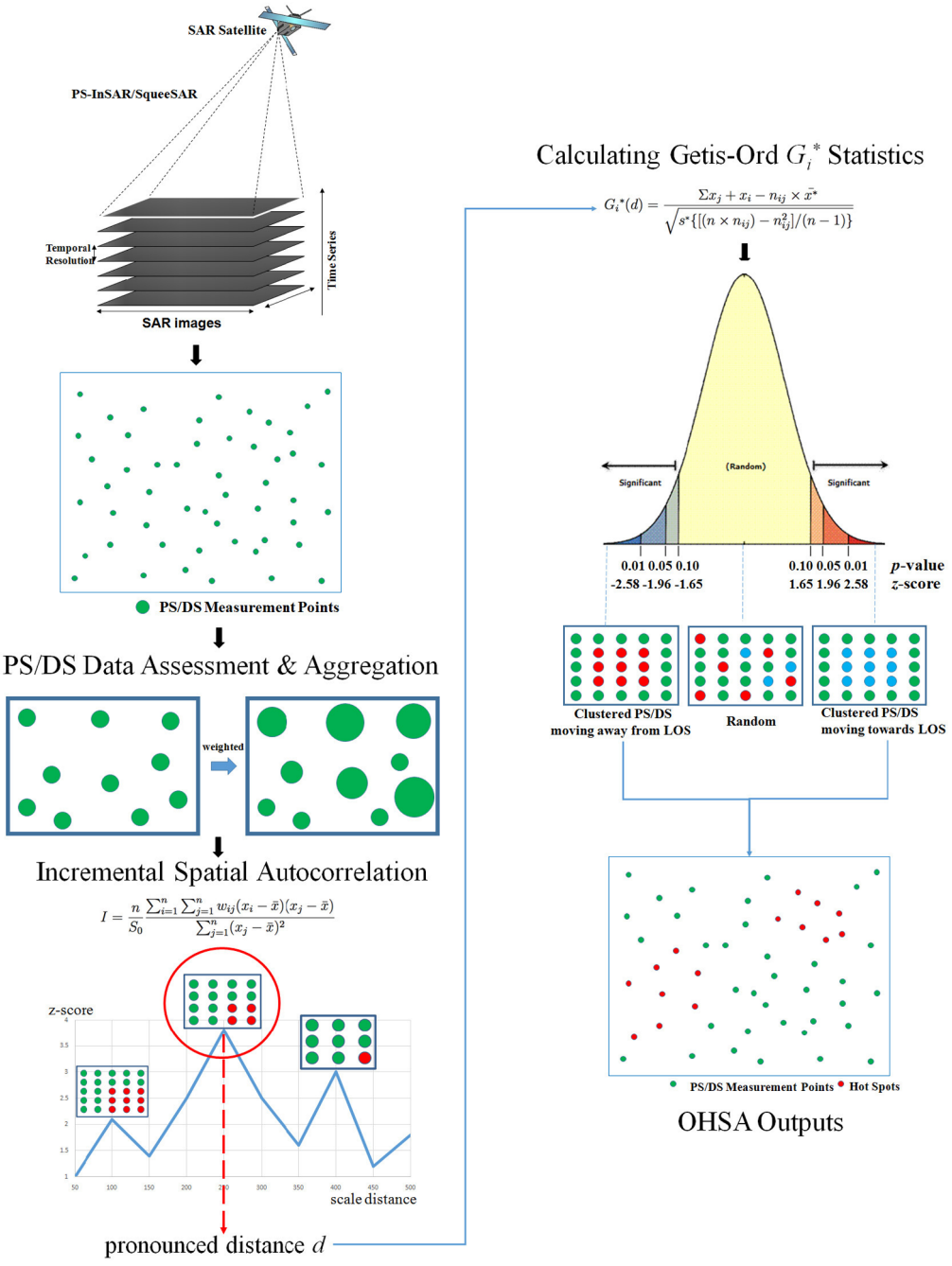

Fig. 2. The flowchart of OHSA on PS/DS MP.

infrastructures and roads, PS/DS MP are also recognized in rural vegetated areas around Volterra. An overview of the derived PS/DS MP extracted from the COSMO-SkyMed scenes is demonstrated in Fig. 4.

The OHSA approach has extracted 154 and 283 HS from ascending and descending ENVISAT PS, respectively. The output of OHSA from ENVISAT PS rendered on the landslide inventory is illustrated in Fig. 5.

In terms of Cosmo-SkyMed PS/DS MP, in Volterra the OHSA approach has derived 844 and 942 HS from the ascending and descending orbits, respectively. An overview of the Cosmo-SkyMed HS across the urban Volterra area is displayed in Fig. 6.

The result of the accuracy assessment of PS/DS and HS for landslide detection in the Volterra area is summarized in Table 2. Both detection accuracy and redundancy were evaluated. The detection accuracy is measured as the percentage of active PS/DS MP and HS detected inside landslides. The redundancy is calculated as the number of active PS/DS MP and HS detected outside landslides divided by the total number of PS/DS MP outside landslides.

For PS datasets processed from ENVISAT images by PS-InSAR, the landslide detection accuracies for descending and ascending orbits are 50.7% and 23.3%, respectively, with both 5.3% redundancies. When OHSA is implemented, the landslide detection accuracies for descending and ascending PS datasets can be increased to 66.4% and 25.3%, with corresponding redundancy decreased to 2.4% and 3.7%, respectively.

For PS/DS datasets acquired from COSMO-SkyMed images using the SqueeSAR technique, the landslide detection accuracies for descending and ascending orbits are 73.8% and 57.7%, with redundancy of 3.4% and 3.1%, respectively. When OHSA is applied, the landslide detection accuracies for descending and ascending PS/DS datasets can be increased to 81.5% and 70.3%, with decreased redundancy of 2.1% and

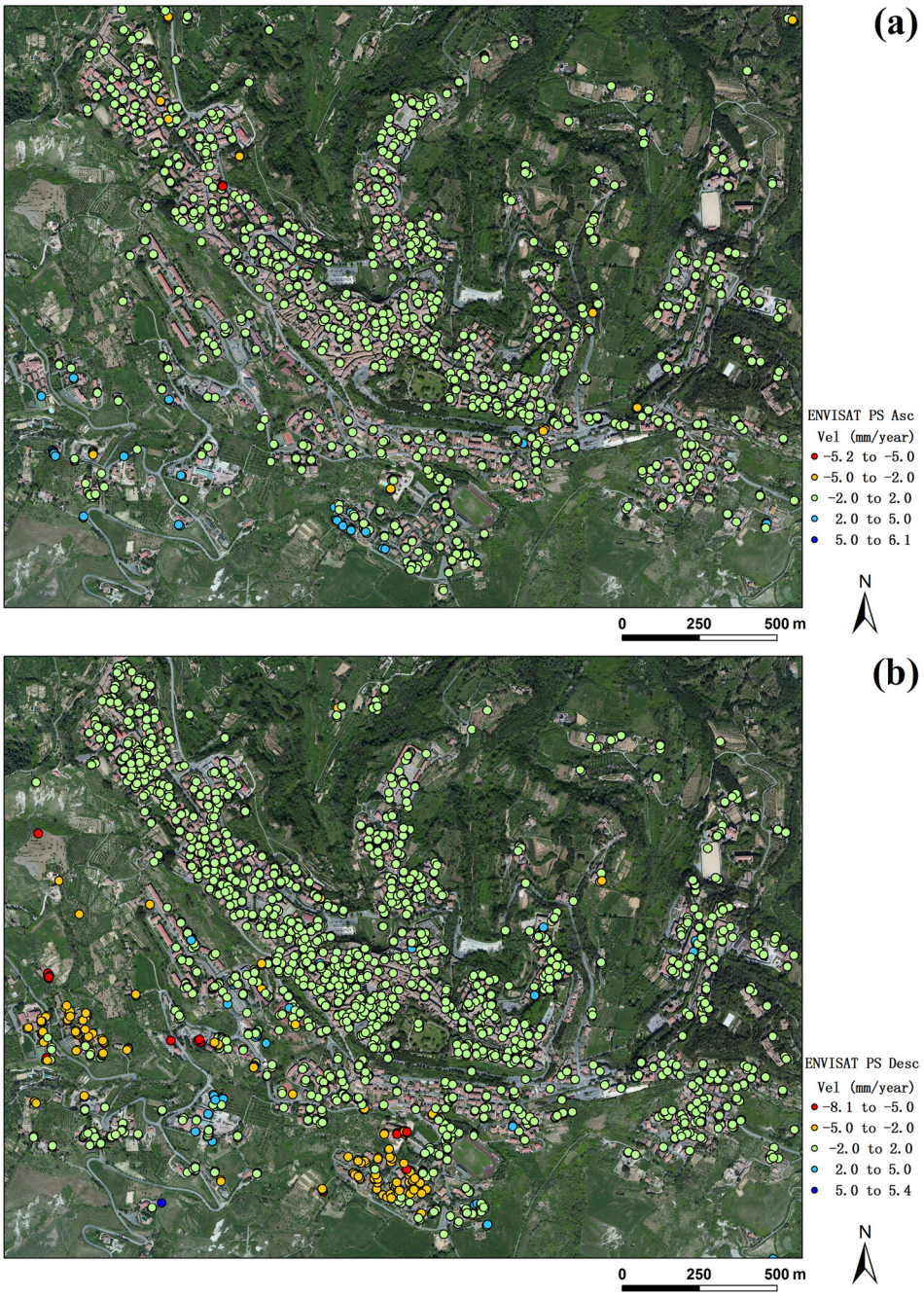

Fig. 3. PS extracted by PS-InSAR from the C-band ENVISAT imageries in Volterra: (a) ascending and (b) descending orbit.

1.7%, respectively.

In consequence, it can be seen from the results that, (1) when OHSA is implemented, the accuracy for landslide detection can be improved; (2) the landslide detection accuracy for COSMO-SkyMed PS/DS datasets by SqueeSAR is better than that for ENVISAT PS datasets based on PS-InSAR; (3) OHSA-derived HS achieve improved redundancy compared to PS/DS MP.

5. Discussion

For both PS extracted from ENVISAT by PS-InSAR and PS/DS achieved from COSMO-SkyMed by SqueeSAR, higher landslide detection accuracies have been achieved by deployment of OHSA. This result indicates the usefulness of the proposed method for effective landslide detection. Such advantage of OHSA may be primarily attributed to two factors. Firstly, spatial clustering is able to describe the excess of events or values in geographic space with higher or lower spatial densities (Jacquez, 2008), and OHSA is precisely the approach that utilized the Getis-Ord G_i^* statistics to analyze this spatial clustering tendency in PS and DS velocities that have this clustering nature. These long-term InSAR scatterers can often be collectively identified in homogeneous areas or infrastructures where uniform pattern of topography, geomorphology, texture and land cover may exist. In addition, if coherence remains high, a group of PS and DS can be identified on individual object and they may display similar velocity patterns, thus appearing to be spatially clustered. Secondly, in terms of landslides, they may also have the clustering tendency in space. Landslides appear to occur in or near the specific places where they may have occurred in the past and accordingly can be spatially discontinuous and mapped in cluster (Malamud et al., 2004; Bertolini et al., 2005; Lu et al., 2019). Also, even

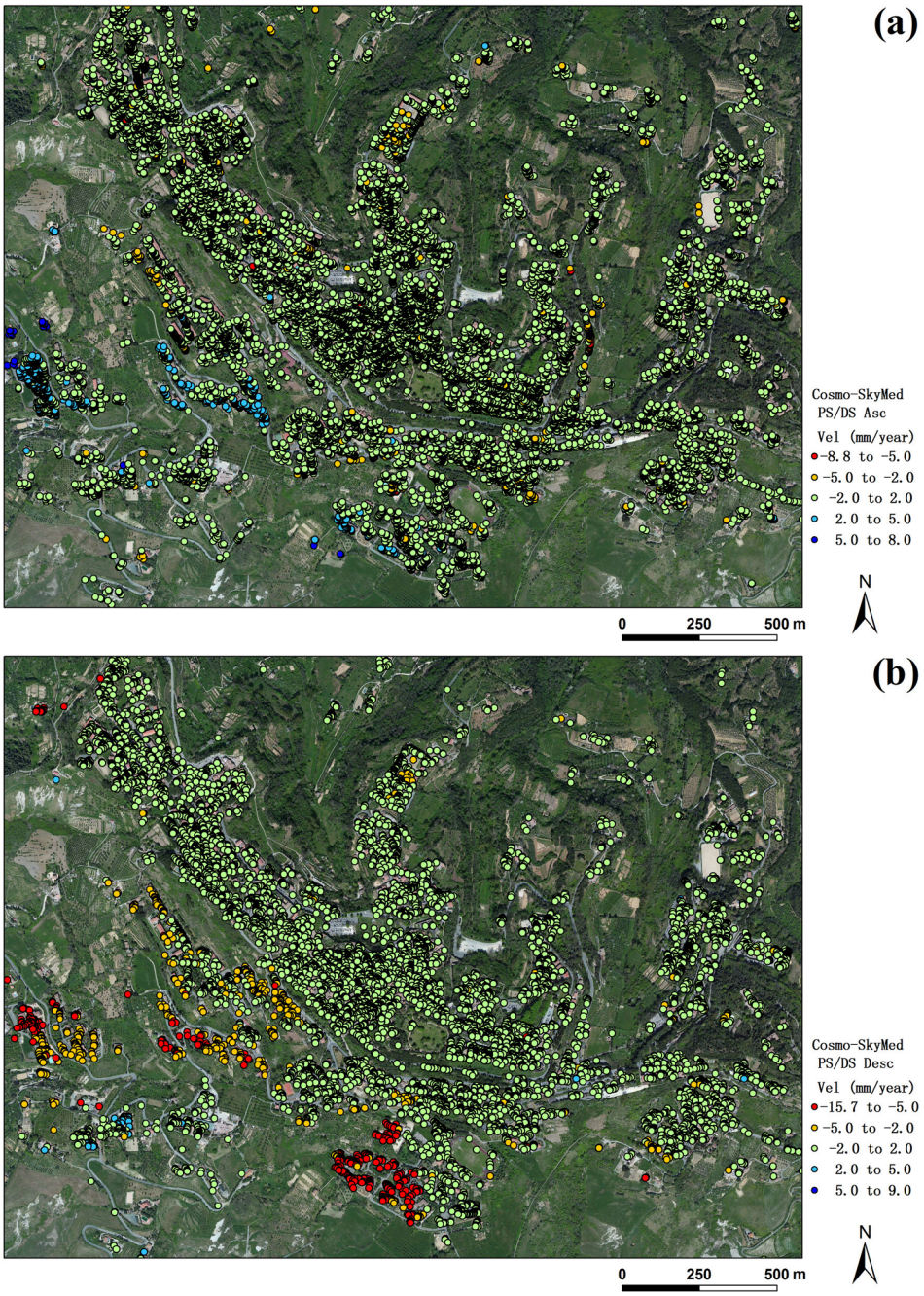

Fig. 4. PS/DS MP extracted by SqueeSAR from the X-band COSMO-SkyMed imageries in Volterra: (a) ascending and (b) descending orbit.

for a small landslide, the spatial extent is large enough to cover a group of PS and DS MP, and if parts of landslide show uniform movements and temporal coherence remains high, spatial clustering may exist and represent such consistent mass movement. Therefore, the existence of group of landslides can also be suggested by the spatial clustering analysis of PS and DS MP, such as OHSA. Namely, OHSA can recognize statistically significant spatial clusters of PS/DS MP of high velocities for the purpose of landslide detection.

Lu et al. (2012) deployed a spatial clustering analysis on RADARSAT-1 PS for landslide detection through PSI-HCA, a method also based on the Getis-Ord G_i^* statistics. Although PSI-HCA has been proven effective, the scale distance of analysis was determined by a complex way: (1) a 10 m DTM was firstly generated from the topographic map, (2) then for each pixel of DTM the average distance of the shortest distances to channel and ridge was calculated based on the approach proposed by Tucker et al. (2001), and (3) finally a kernel density estimation was performed based on the z-score of each PS and the scale distance needs to be defined again in this step. Finally, for an advanced understanding of the impact of scale distance on landslide clustering, an additional bivariate K-function analysis on spatial relationships between PS and landslides is suggested for PSI-HCA (Lu et al., 2014b). PSI-HCA has the advantage that the scale distance for spatially clustering can be determined from topography and the sum of the shortest distances to a channel and a ridge can be used as a proxy for the limiting dimension of a landslide over hillslope. However, this approach is relatively complicated and fundamentally needs a DTM with decent resolution that may often be unavailable over a large area. Compared to PSI-HCA, OHSA nevertheless estimates the optimal HS of PS/DS MP by determining a pronounced scale through the peak distance of incremental spatial autocorrelation. As a result, OHSA is an ordinary

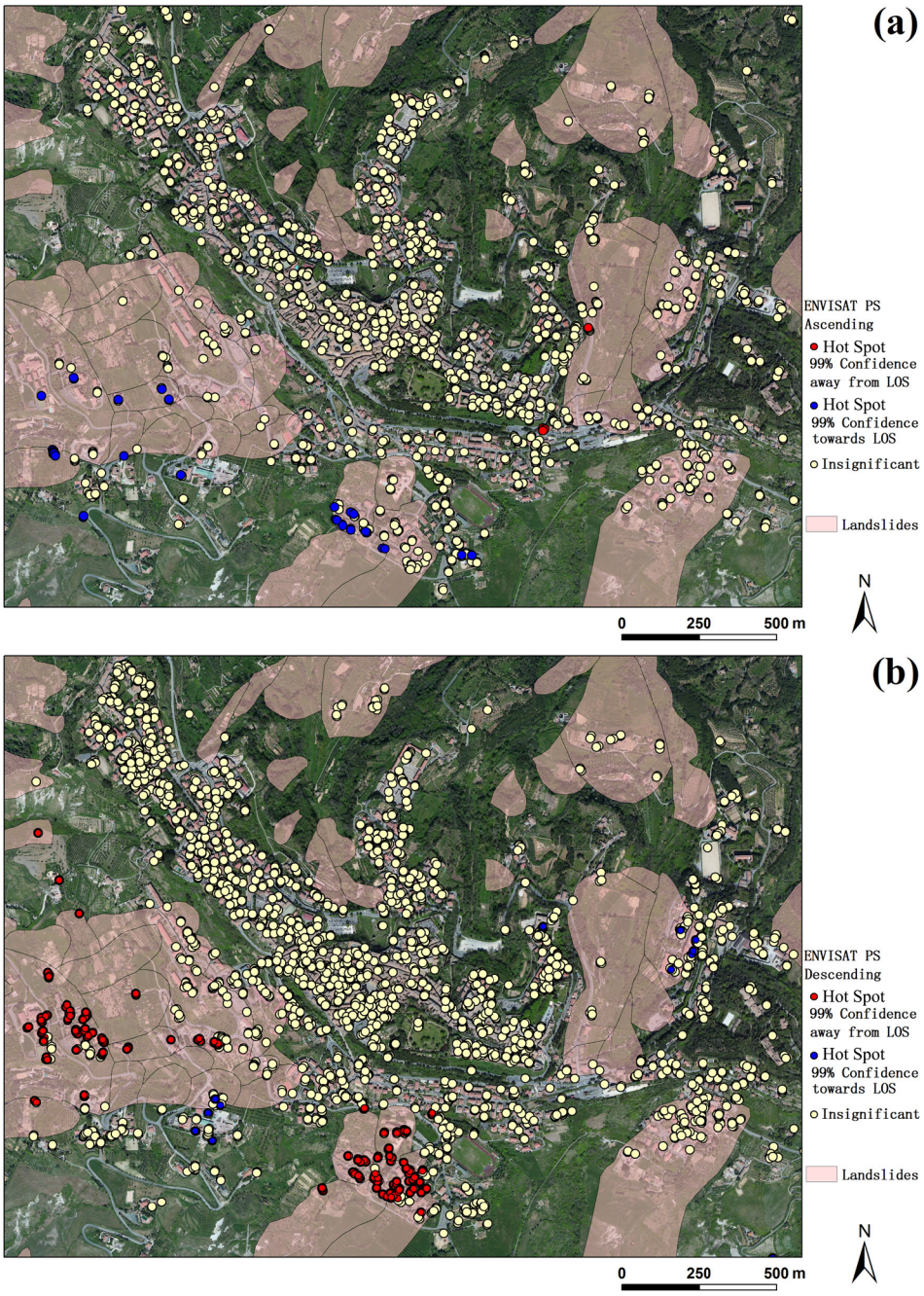

Fig. 5. HS derived by OHSA from ENVISAT in urban Volterra area: (a) ascending and (b) descending HS map. A manually prepared landslide inventory is also displayed.

approach that can be easily implemented in a wide study area without the need for a DTM, and an efficient method that can automatically estimate the optimal HS from PS and DS.

The landslide detection accuracy for COSMO-SkyMed PS/DS MP processed from SqueeSAR is better than ENVISAT PS processed exclusively from PS-InSAR. This may be attributed to (1) the processing approach of SqueeSAR and (2) the sensor of COSMO-SkyMed.

Firstly, SqueeSAR is an advanced long-term InSAR approach that was furthered developed from PS-InSAR. The outcomes of PS-InSAR and SqueeSAR are PS and PS/DS MP, respectively. PS are point-wise coherent scatterers whereas DS are partially coherent scatterers that correspond to a set of pixels (Carlà et al., 2016). Better landslide detection accuracy achieved by SqueeSAR than PS-InSAR can be attributed to the differences in the data processing algorithms as mentioned in Ferretti et al. (2011): (1) PS-InSAR utilizes a subset of interferograms while SqueeSAR employs all possible interferograms to assess the optimal phase values using the coherence matrix without a consideration of temporal and geometrical baseline; (2) SqueeSAR is less dependent on phase unwrapping than PS-InSAR due to the fact that optimal phase values are combined and reconstructed before phase unwrapping; and (3) SqueeSAR is less affected by the filtering process since only pixels that are statistically homogeneous are averaged. These three characteristics ensure the density and quality of SqueeSAR outcomes. For example, PS are mainly recognized as man-made objects such as buildings, infrastructures, roads, outcrops etc., whereas DS often represent homogeneous ground surfaces such as uncultivated, desert or debris covered areas (Lagios et al., 2013). In consequence, due to the improved density and quality, SqueeSAR facilitates the utilization of

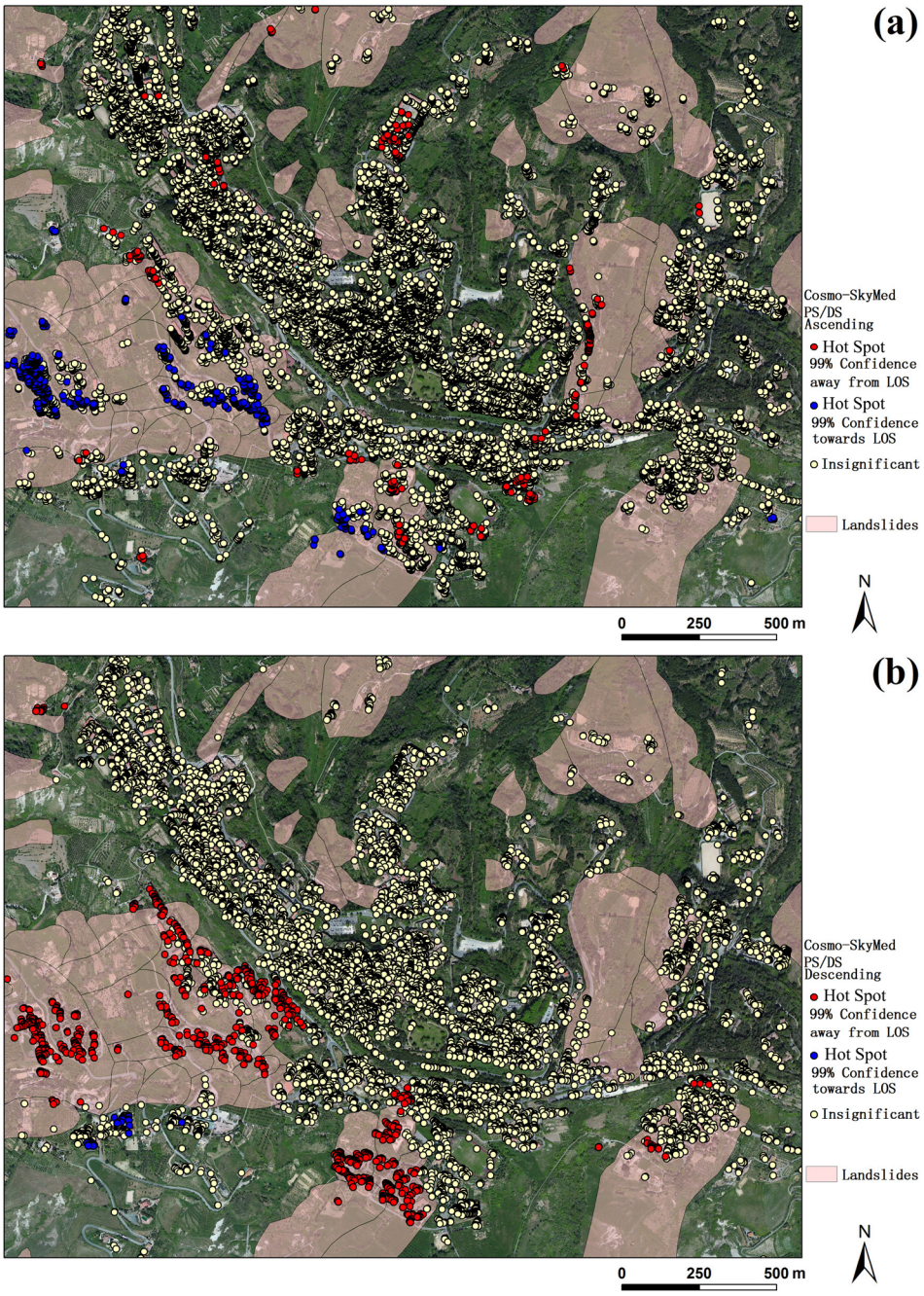

Fig. 6. HS derived by OHSA from Cosmo-SkyMed PS/DS MP in the urban Volterra area: (a) ascending and (b) descending HS map. A manually prepared landslide inventory is also displayed.

InSAR in non-urban areas affected by landslide hazards, thus enhancing the usefulness of PS/DS in landslide detection. Furthermore, the utilized SqueeSAR technique chiefly concentrates on pixels in areas of moderate coherence, where surrounding pixels appear to contribute homogeneous reflectivity values as they belong to the same object (Crosetto et al., 2016). For a better description of these characteristics, Fig. 7 displays the outcomes of both PS-InSAR and SqueeSAR over a detected landslide-affected area of Il Cipresso. The SqueeSAR technique has already pre-defined those statistically homogeneous areas by selecting a group of statistically homogeneous pixels (SHP) through the KS test, which is based on the maximum absolute difference between two cumulative distribution functions (Ferretti et al., 2011). Alternatively speaking, homogeneous pixels of DS have already been previously clustered by comparing with their neighbors during this KS test. Therefore, the SqueeSAR outcomes are prone to be further identified as clustered HS and thus more applicable for OHSA.

Secondly, the X-band COSMO-SkyMed sensor has improved spatial resolution over the C-band ENVISAT satellite. The advantage of the X-band COSMO-SkyMed over the C-band ENVISAT satellite is chiefly reflected in the increase of total number of scatterers that can be identified in the landslide-affected areas and is therefore more suitable for OHSA. A number of studies have already demonstrated that higher PS density can be achieved in both urban and suburban areas using the X-band images. For example, Bovenga et al. (2012) have acquired PS density up to 11 times higher from the X-band COSMO-SkyMed images than the C-band ENVISAT products for landslide hazard assessment. Similar study conducted by Herrera et al. (2010) estimated that such difference is about 10 times in the Vega Media of the Segura River

Table 2
Accuracy assessment for landslides detection from PS/DS MP and HS.

	No. of active MP/HS	No. of active MP/HS inside landslides	No. of active MP/HS outside landslides	Total No. of MP outside landslides	Detection accuracy	Redundancy
MP/HS from COSMO-SkyMed by SqueeSAR						
PS/DS – COSMO-SkyMed Descending	1082	799	283	8341	73.8%	3.4%
HS – COSMO-SkyMed Descending	942	768	174	8341	81.5%	2.1%
PS/DS – COSMO-SkyMed Ascending	1120	646	474	15,076	57.7%	3.1%
HS – COSMO-SkyMed Ascending	844	593	251	15,076	70.3%	1.7%
MP/HS from ENVISAT by PS-InSAR						
PS – ENVISAT Descending	428	217	211	3997	50.7%	5.3%
HS – ENVISAT Descending	283	188	95	3997	66.4%	2.4%
PS – ENVISAT Ascending	215	50	165	3089	23.3%	5.3%
HS – ENVISAT Ascending	154	39	115	3089	25.3%	3.7%

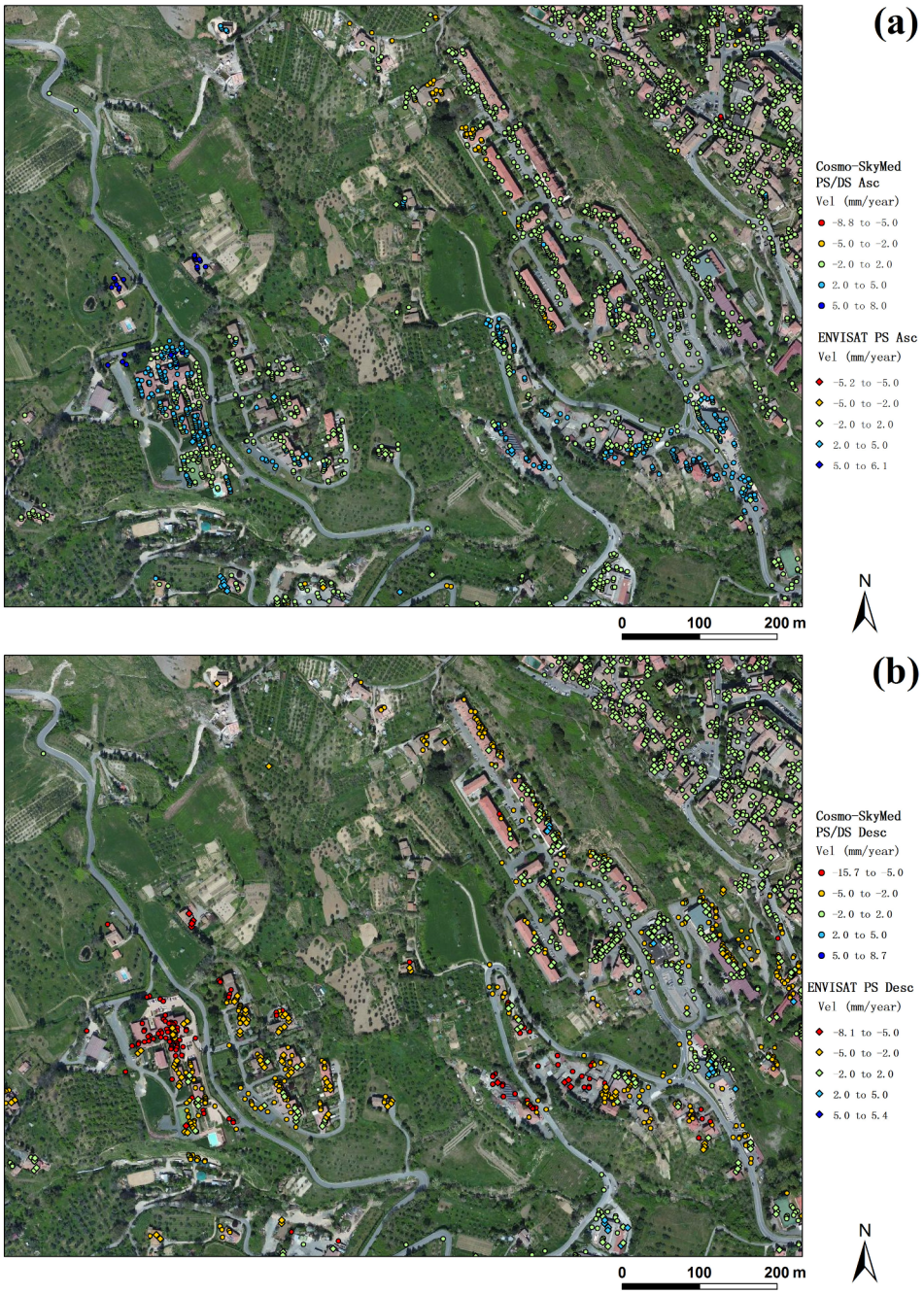

Fig. 7. The spatial distribution of ENVISAT PS and Cosmo-SkyMed PS/DS MP in a detected landslide-affected area of Il Cipresso from (a) ascending and (b) descending orbit.

(Spain) for subsidence monitoring. Moreover, Crosetto et al. (2010) have shown that such increase for COSMO-SkyMed may reach to 47 times higher than ENVISAT in urban areas. Cigna et al. (2014) have estimated that in each acquisition mode scatterers obtained from COSMO-SkyMed is about 25 million more than those from C-band satellites. Thus, in terms of point density, it appears that X-band satellites are more suitable for OSHA than C-band images. However, this does not mean that C-band satellites are less applicable for OHSA, especially considering that some C-band sensors, such as the spotlight beam mode of RADARSAT-2, may also provide sufficient spatial resolution. In addition, the improved temporal resolution of COSMO-SkyMed facilitates to recognize faster mass movements than ENVISAT and may identify more scatterers for OHSA. Future research is suggested to focus on C-band Sentinel-1 images, which offers a repeat cycle of six days through the two-satellite constellation and may accordingly have great potential in OHSA.

The redundancy was mainly used to estimate the performance of OHSA outside the landslide inventory in terms of detection efficiency. However, it may not thoroughly justify the landslide detection accuracy as revealed by these active PS/DS and HS datasets. On one hand, such active mass movements may be related to landslide activities that were not recorded in the current landslide inventory; namely, the landslide inventory may be incomplete. On the other hand, those ground movements may be related to other geo-processes such as subsidence, sinkholes, building consolidations, tectonics and underground works for downward movements, and fluid injection, sedimentation of rivers and tectonics for upward movements (Lu et al., 2012). As a result, further intensive investigations particularly with detailed field surveys are valuable for a thorough understanding of the actual ground motions that represented by those active PS/DS and HS datasets.

6. Conclusion

This study proposed a novel approach of OHSA on PS and DS datasets and subsequently evaluated its potential in landslide detection across the Volterra area. Firstly, PS processed from eight years (2003–2010) of ENVISAT images were acquired by PS-InSAR, and PS/DS MP processed from four years (2011–2014 for ascending and 2010–2013 for descending orbit) of COSMO-SkyMed images were obtained by SqueeSAR. Secondly, the OHSA approach was employed on the derived PS and DS datasets in order to analyze their spatial clustering tendencies, consequently rendering the calculated values of z-score (standard deviation) and p-value (independence probability) for estimating their statistical significance of spatial autocorrelation. Thirdly, a landslide inventory covering the Volterra area was manually prepared as the reference data for accuracy assessment of landslide detection.

The results indicate that in the Volterra area a total of 215 and 428 active ENVISAT PS has been derived by PS-InSAR for ascending and descending orbits, respectively. In addition, 1120 and 1082 active COSMO-SkyMed PS/DS MP have been acquired by SqueeSAR from ascending and descending imageries, respectively. After the implementation of OHSA, PS/DS datasets with velocity $>|\pm 2|$ mm/year, p-value < 0.01 and z-score $>|\pm 2.58|$ were identified as HS. 154 and 283 HS have been extracted from the ascending and descending ENVISAT PS, respectively. Also, 844 and 942 HS have been acquired from the ascending and descending Cosmo-SkyMed imageries, respectively. In terms of landslide detection, for OHSA-derived ENVISAT HS, the detection accuracy can be increased from 50.7% to 66.4% and from 23.3% to 25.3%, with decreased redundancy from 5.3% to 3.7% and from 5.3% to 2.4%, for ascending and descending datasets, respectively. For OHSA-derived Cosmo-SkyMed HS, the detection accuracy can be improved from 57.7% to 70.3% and from 73.8% to 81.5%, with decreased redundancy from 3.1% to 1.7% and from 3.4% to 2.1%, for ascending and descending orbits, respectively.

Compared to traditional HS analysis such as PSI-HCA, OHSA is compelling considering that the scale distance used for the Getis-Ord G_i^* statistics can be automatically determined without manual intervention or the need for an additional DTM. Furthermore, The proposed method is succinct and can be easily implemented in diverse GIS platforms. In consequence, the proposed approach has great potential in rapid detection of landslide hazards over a wide area. Finally, to the best of our knowledge, it is the first time that OHSA has been applied to PS and DS datasets.

Acknowledgments

This study was funded by the National Key R&D Program of China (2017YFA0603100), National Natural Science Foundation of China (No. 41671413), the Opending Fund of Key Laboratory of Mountain Surface Process and Hazards of CAS (No. KLMHESP-17-07), the IPL project of the International Consortium on Landslides (ICL) and the Fundamental Research Funds for the Central Universities (Tongji University).

References

Bamler, R., Hartl, P., 1998. Synthetic aperture radar interferometry. Inverse Probl. 14 (4), R1.
Bayer, B., Schmidt, D., Simoni, A., 2017. The influence of external digital elevation models on PS-InSAR and SBAS results: implications for the analysis of deformation signals caused by slow moving landslides in the Northern Apennines (Italy). IEEE Trans. Geosci. Remote Sens. 55 (5), 2618–2631.
Bazzoffi, P., Boscagli, A., Brandi, G., Busoni, E., Calzolari, C., Chiarucci, A., Chiaverini, I., Chisci, G., Colica, A., De Dominicis, V., et al., 1997. Badland processes and significance in changing environments. Supplementi di Geografia Fisica e Dinamica del Quaternario 3, 151–166.
Bertolini, G., Guida, M., Pizziolo, M., 2005. Landslides in Emilia-Romagna region (Italy): strategies for hazard assessment and risk management. Landslides 2 (4), 302–312.
Bianchini, S., Herrera, G., Mateos, R.M., Notti, D., Garcia, I., Mora, O., Moretti, S., 2013. Landslide activity maps generation by means of persistent scatterer interferometry. Remote Sens. 5 (12), 6198–6222.
Bianchini, S., Ciampalini, A., Raspini, F., Bardi, F., Di Traglia, F., Moretti, S., Casagli, N., 2015a. Multi-temporal evaluation of landslide movements and impacts on buildings in San Fratello (Italy) By Means of C-Band and X-Band PSI Data. Pure Appl. Geophys. 172 (11), 3043–3065.
Bianchini, S., Pratesi, F., Nolesini, T., Casagli, N., 2015b. Building deformation assessment by means of Persistent Scatterer Interferometry analysis on a landslide-affected area: the Volterra (Italy) case study. Remote Sens. 7 (4), 4678–4701.
Bianchini, S., Del Soldato, M., Solari, L., Nolesini, T., Pratesi, F., Moretti, S., 2016. Badland susceptibility assessment in Volterra municipality (Tuscany, Italy) by means of GIS and statistical analysis. Environ. Earth Sci. 75 (10), 1–14.
Blanco-Sanchez, P., Mallorqui, J., Duque, S., Monells, D., 2008. The Coherent Pixels Technique (CPT): An advanced DInSAR technique for nonlinear deformation monitoring. Pure Appl. Geophys. 165 (6), 1167–1193.
Bouali, E., Oommen, T., Escobar-Wolf, R., 2018. Mapping of slow landslides on the Palos Verdes Peninsula using the California landslide inventory and persistent scatterer interferometry. Landslides 15 (3), 439–452.
Bovenga, F., Wasowski, J., Nitti, D.O., Nutricato, R., Chiaradia, M.T., 2012. Using COSMO/SkyMed X-band and ENVISAT C-band SAR interferometry for landslides analysis. Remote Sens. Environ. 119, 272–285.
Canuti, P., Casagli, N., Ermini, L., Fanti, R., Farina, P., 2002. Landslide activity as a geoindicator in Italy: significance and new perspectives from remote sensing. Environ. Geol. 45 (7), 907–919.
Carlà, T., Raspini, F., Intrieri, E., Casagli, N., 2016. A simple method to help determine landslide susceptibility from spaceborne InSAR data: the Montescaglioso case study. Environ. Earth Sci. 75 (24), 1492.
Ciampalini, A., Bardi, F., Bianchini, S., Frodella, W., Del Ventisette, C., Moretti, S., Casagli, N., 2014. Analysis of building deformation in landslide area using multisensor PSInSAR technique. Int. J. Appl. Earth Obs. Geoinf. 33, 166–180.
Ciampalini, A., Raspini, F., Lagomarsino, D., Catani, F., Casagli, N., 2016. A simple method to help determine landslide susceptibility from spaceborne InSAR data: the Montescaglioso case studyLandslide susceptibility map refinement using PSInSAR data. Remote Sens. Environ. 184, 302–315.
Cigna, F., Bianchini, S., Casagli, N., 2013. How to assess landslide activity and intensity

with Persistent Scatterer Interferometry (PSI): the PSI-based matrix approach. Landslides 10 (3), 267–283.
Cigna, F., Bateson, L.B., Jordan, C.J., Dashwood, C., 2014. Simulating SAR geometric distortions and predicting Persistent Scatterer densities for ERS-1/2 and ENVISAT C-band SAR and InSAR applications: Nationwide feasibility assessment to monitor the landmass of Great Britain with SAR imagery. Remote Sens. Environ. 152, 441–466.
Colesanti, C., Ferretti, A., Prati, C., Rocca, F., 2003. Landslide activity as a geoindicator in Italy: significance and new perspectives from remote sensing. Eng. Geol. 68 (1–2), 3–14.
Colesanti, C., Wasowski, J., 2006. Investigating landslides with space-borne synthetic aperture radar (SAR) Interferometry. Eng. Geol. 88 (3–4), 173–199.
Confuorto, P., Di Martire, D., Centolanza, G., Iglesias, R., Mallorqui, J.J., Novellino, A., Plank, S., Ramondini, M., Thuro, K., Calcaterra, D., 2017. Post-failure evolution analysis of a rainfall-triggered landslide by multi-temporal interferometry SAR approaches integrated with geotechnical analysis. Remote Sens. Environ. 188, 51–72.
Crosetto, M., Biescas, E., Duro, J., Closa, J., Arnaud, A., 2008. Generation of advanced ERS and Envisat interferometric SAR products using the stable point network technique. Photogram. Eng. Remote Sens. 74 (4), 443–450.
Crosetto, M., Monserrat, O., Iglesias, R., Crippa, B., 2010. Persistent scatterer interferometry: potential, limits and initial C- and X-band comparison. Photogram. Eng. Remote Sens. 76 (9), 1061–1069.
Crosetto, M., Monserrat, O., Cuevas-Gonzalez, M., Devanthery, N., Crippa, B., 2016. Persistent scatterer interferometry: a review. ISPRS J. Photogram. Remote Sens. 115, 78–89.
Delgado, J., Vicente, F., Garcia-Tortosa, F., Alfaro, P., Estevez, A., Lopez-Sanchez, J.M., Tomas, R., Mallorqui, J.J., 2011. A deep seated compound rotational rock slide and rock spread in SE Spain: structural control and DInSAR monitoring. Geomorphology 129 (3–4), 252–262.
Dong, J., Zhang, L., Tang, M., Liao, M., Xu, Q., Gong, J., Ao, M., 2018. Mapping landslide surface displacements with time series SAR interferometry by combining persistent and distributed scatterers: a case study of Jiaju landslide in Danba, China. Remote Sens. Environ. 205, 180–198.
ESRI, 2017. How Optimized Hot Spot Analysis Works. <http://desktop.arcgis.com/en/arcmap/10.7/tools/spatial-statistics-toolbox/how-optimized-hot-spot-analysis-works.htm> (accessed 17 April 2018).
Ferretti, A., Prati, C., Rocca, F., 2000. Nonlinear subsidence rate estimation using Permanent Scatterers in differential SAR Interferometry. IEEE Trans. Geosci. Remote Sens. 38 (5), 2202–2212.
Ferretti, A., Prati, C., Rocca, F., 2001. Permanent scatterers in SAR interferometry. IEEE Trans. Geosci. Remote Sens. 39 (1), 8–20.
Ferretti, A., Fumagalli, A., Novali, F., Prati, C., Rocca, F., Rucci, A., 2011. A new algorithm for processing interferometric data-stacks: SqueeSAR. IEEE Trans. Geosci. Remote Sens. 49 (9), 3460–3470.
Getis, A., Ord, J.K., 1992. The analysis of spatial association by use of distance statistics. Geogr. Anal. 24 (3), 189–206.
Getis, A., Ord, J.K., 1996. Local spatial statistics: an overview. In: Longley, P., Batty, M. (Eds.), Spatial Analysis: Modelling in A GIS Environment. John Wiley & Sons Inc., pp. 261–277.
Greif, V., Vlcko, J., 2012. Monitoring of post-failure landslide deformation by the PS-InSAR technique at Lubietova in Central Slovakia. Environ. Earth Sci. 66 (6), 1585–1595.
Guzzetti, F., 2000. Landslide fatalities and the evaluation of landslide risk in Italy. Eng. Geol. 58 (2), 89–107.
Guzzetti, F., Tonelli, G., 2004. Information system on hydrological and geomorphological catastrophes in Italy (SICI): a tool for managing landslide and flood hazards. Nat. Hazards Earth Syst. Sci. 4 (2), 213–232.
Hanssen, R.F., 2001. Radar Interferometry: Data Interpretation and Error Analysis (Vol. 2). Kluwer Academic Publishers, Dordrecht, The Netherlands.
Herrera, G., Davalillo, J.C., Mulas, J., Cooksley, G., Monserrat, O., Pancioli, V., 2009. Mapping and monitoring geomorphological processes in mountainous areas using PSI data: Central Pyrenees case study. Nat. Hazards Earth Syst. Sci. 9 (5), 1587–1598.
Herrera, G., Tomas, R., Monells, D., Centolanza, G., Mallorqui, J.J., Vicente, F., Navarro, V.D., Lopez-Sanchez, J.M., Sanabria, M., Cano, M., Mulas, J., 2010. Analysis of subsidence using TerraSAR-X data Murcia case study. Eng. Geol. 116 (3–4), 284–295.
Herrera, G., Notti, D., Carlos Garcia-Davalillo, J., Mora, O., Cooksley, G., Sanchez, M., Arnaud, A., Crosetto, M., 2011. Analysis with C- and X-band satellite SAR data of the Portalet landslide area. Landslides 8 (2), 195–206.
Herrera, G., Gutierrez, F., Garcia-Davalillo, J.C., Guerrero, J., Notti, D., Galve, J.P., Fernandez-Merodo, J.A., Cooksley, G., 2013. Multi-sensor advanced DInSAR monitoring of very slow landslides: the Tena Valley case study (Central Spanish Pyrenees). Remote Sens. Environ. 128, 31–43.
Hilley, G.E., Burgmann, R., Ferretti, A., Novali, F., Rocca, F., 2004. Dynamics of slow-moving landslides from permanent scatterer analysis. Science 304 (5679), 1952–1955.
Hooper, A., Zebker, H., Segall, P., Kampes, B., 2004. A new method for measuring deformation on volcanoes and other natural terrains using InSAR Persistent Scatterers. Geophys. Res. Lett. 31 (23).
Hooper, A., Segall, P., Zebker, H., 2007. Persistent scatterer interferometric synthetic aperture radar for crustal deformation analysis, with application to Volcan Alcedo, Galapagos. J. Geophys. Res.-Solid Earth 112 (B7).
Hu, J., Li, Z.W., Ding, X.L., Zhu, J.J., Zhang, L., Sun, Q., 2014. Resolving three-dimensional surface displacements from InSAR measurements: a review. Earth Sci. Rev. 133, 1–17.
Intrieri, E., Raspini, F., Fumagalli, A., Lu, P., Del Conte, S., Farina, P., Allievi, J., Ferretti, A., Casagli, N., 2018. The Maoxian landslide as seen from space: detecting precursors of failure with Sentinel-1 data. Landslides 15 (1), 123–133.
Jacquez, G., 2008. Spatial cluster analysis. In: Fotheringham, S., Wilson, J. (Eds.), The Handbook of Geographic Information Science. Blackwell Publishing, pp. 395–416.
Lagios, E., Sakkas, V., Novali, F., Bellotti, F., Ferretti, A., Vlachou, K., Dietrich, V., 2013. SqueeSAR (TM) and GPS ground deformation monitoring of Santorini Volcano (1992–2012): tectonic implications. Tectonophysics 594, 38–59.
Lauknes, T.R., Shanker, A., Dehls, J.F., Zebker, H.A., Henderson, I.H.C., Larsen, Y., 2010. Detailed rockslide mapping in northern Norway with small baseline and persistent scatterer interferometric SAR time series methods. Remote Sens. Environ. 114 (9), 2097–2109.
Liu, G., Jia, H., Nie, Y., Li, T., Zhang, R., Yu, B., Li, Z., 2014. Detecting subsidence in coastal areas by ultrashort-baseline TCPInSAR on the Time Series of High-Resolution TerraSAR-X Images. IEEE Trans. Geosci. Remote Sens. 52 (4), 1911–1923.
Lu, P., Casagli, N., Catani, F., Tofani, V., 2012. Persistent scatterers interferometry hotspot and cluster analysis (PSI-HCA) for detection of extremely slow-moving landslides. Int. J. Remote Sens. 33 (2), 466–489.
Lu, P., Catani, F., Tofani, V., Casagli, N., 2014a. Quantitative hazard and risk assessment for slow-moving landslides from Persistent Scatterer Interferometry. Landslides 11 (4), 685–696.
Lu, P., Bai, S., Casagli, N., 2014b. Investigating spatial patterns of persistent scatterer interferometry point targets and landslide occurrences in the Arno River Basin. Remote Sens. 6 (8), 6817–6843.
Lu, P., Qin, Y., Li, Z., Mondini, A.C., Casagli, N., 2019. Landslide mapping from multi-sensor data through improved change detection-based Markov random field. Remote Sens. Environ. 231, 111235.
Malamud, B.D., Turcotte, D.L., Guzzetti, F., Reichenbach, P., 2004. Landslide inventories and their statistical properties. Earth Surf. Proc. Land. 29 (6), 687–711.
Massonnet, D., Feigl, K.L., 1998. Radar interferometry and its application to changes in the Earth's surface. Rev. Geophys. 36 (4), 441–500.
Mora, O., Mallorqui, J.J., Broquetas, A., 2003. Linear and nonlinear terrain deformation maps from a reduced set of interferometric SAR images. IEEE Trans. Geosci. Remote Sens. 41 (10), 2243–2253.
Nolesini, T., Frodella, W., Bianchini, S., Casagli, N., 2016. Detecting slope and urban potential unstable areas by means of multi-platform remote sensing techniques: the Volterra (Italy) Case Study. Remote Sens. 8 (9), 746.
Notti, D., Davalillo, J.C., Herrera, G., Mora, O., 2010. Assessment of the performance of X-band satellite radar data for landslide mapping and monitoring: Upper Tena Valley case study. Nat. Hazards Earth Syst. Sci. 10 (9), 1865–1875.
Notti, D., Herrera, G., Bianchini, S., Meisina, C., Carlos Garcia-Davalillo, J., Zucca, F., 2014. A methodology for improving landslide PSI data analysis. Int. J. Remote Sens. 35 (6), 2186–2214.
Notti, D., Galve, J.P., Mateos, R.M., Monserrat, O., Lamas-Fernndez, F., Fernandez-Chacon, F., Roldan-Garcia, F.J., Perez-Pena, J.V., Crosetto, Mi, Azanon, J.M., 2015. Human-induced coastal landslide reactivation. Monitoring by PSInSAR techniques and urban damage survey (SE Spain). Landslides 12 (5), 1007–1014.
Oliveira, S.C., Zezere, J.L., Catalao, J., Nico, G., 2015. The contribution of PSInSAR interferometry to landslide hazard in weak rock-dominated areas. Landslides 12 (4), 703–719.
Ord, J.K., Getis, A., 1995. Local spatial autocorrelation statistics - distributional issues and an application. Geogr. Anal. 27 (4), 286–306.
Peeters, A., Zude, M., Kathner, J., Unlu, M., Kanber, R., Hetzroni, A., Gebbers, R., Ben-Gal, A., 2015. GetisOrds hot-and cold-spot statistics as a basis for multivariate spatial clustering of orchard tree data. Comput. Electron. Agric. 111, 140–150.
Pratesi, F., Nolesini, T., Bianchini, S., Leva, D., Lombardi, L., Fanti, R., Casagli, N., 2015. Early warning GBInSAR-based method for monitoring Volterra (Tuscany, Italy) city walls. IEEE J. Select. Top. Appl. Earth Obser. Remote Sens. 8 (4), 1753–1762.
Raspini, F., Ciampalini, A., Del Conte, S., Lombardi, L., Nocentini, M., Gigli, G., Ferretti, A., Casagli, N., 2015. Exploitation of amplitude and phase of satellite SAR images for landslide mapping: the Case of Montescaglioso (South Italy). Remote Sens. 7 (11), 14576–14596.
Righini, G., Pancioli, V., Casagli, N., 2012. Updating landslide inventory maps using Persistent Scatterer Interferometry (PSI). Int. J. Remote Sens. 33 (7), 2068–2096.
Rosen, P.A., Hensley, S., Joughin, I.R., Li, F., Madsen, S.N., Rodriguez, E., Goldstein, R.M., 2000. Synthetic aperture radar interferometry. Proc. IEEE 88 (3), 333–382.
Rosi, A., Tofani, V., Tanteri, L., Stefanelli, C., Agostini, A., Catani, F., Casagli, N., 2018. The new landslide inventory of Tuscany (Italy) updated with PS-InSAR: geomorphological features and landslide distribution. Landslides 15 (1), 5–19.
Sabelli, R., 2012. Mura etrusche di Volterra: conservazione e valorizzazione. La Grafica Pisana Editrice ISBN, 8897732054.
Sato, A., 2014. Applied Data-Centric Social Sciences: Concepts, Data, Computation, and Theory. Springer ISBN: 9784431549734.
Strozzi, T., Wegmuller, U., Keusen, H.R., Graf, K., Wiesmann, A., 2006. Analysis of the terrain displacement along a funicular by SAR Interferometry. IEEE Geosci. Remote Sens. Lett. 3 (1), 15–18.
Sun, Q., Zhang, L., Ding, X., Hu, J., Li, Z.W., Zhu, J.J., 2015a. Slope deformation prior to Zhouqu, China landslide from InSAR time series analysis. Remote Sens. Environ. 156, 45–57.

Sun, Q., Zhang, L., Ding, X., Hu, J., Liang, H., 2015b. Investigation of slow-moving landslides from ALOS/PALSAR Images with TCPInSAR: a Case Study of Oso, USA. Remote Sens. 7 (1), 72–88.
Sun, Q., Hu, J., Zhang, L., Ding, X., 2016. Towards slow-moving landslide monitoring by integrating multi-sensor InSAR Time Series Datasets: the Zhouqu Case Study, China. Remote Sens. 8 (11), 908.
Terrenato, N., 1998. Tam firmum municipium: the Romanization of Volaterrae and its cultural implications. J. Roman Stud. 88, 94–114.
Tofani, V., Raspini, F., Catani, F., Casagli, N., 2013. Persistent Scatterer Interferometry (PSI) technique for landslide characterization and monitoring. Remote Sens. 5 (3), 1045–1065.
Tucker, G.E., Catani, F., Rinaldo, A., Bras, R.L., 2001. Statistical analysis of drainage density from digital terrain data. Geomorphology 36 (3–4), 187–202.
Werner, C., Wegmuller, U., Strozzi, T., Wiesmann, A., 2003. Interferometric point target analysis for deformation mapping. In: IGARSS 2003 Proceedings, Toulouse France, pp. 4362–4364.
Zhang, L., Lu, Z., Ding, X., Jung, H., Feng, G., Lee, C., 2012. Mapping ground surface deformation using temporarily coherent point SAR interferometry: application to Los Angeles Basin. Remote Sens. Environ. 117, 429–439.